Copy No. 240
RM No. L8G20

NACA

RESEARCH MEMORANDUM

EFFECT OF HIGH-LIFT DEVICES ON THE LOW-SPEED STATIC LATERAL AND YAWING STABILITY CHARACTERISTICS OF AN UNTAPERED 45° SWEPTBACK WING

By

Jacob H. Lichtenstein

Langley Aeronautical Laboratory
Langley Field, Va.

NATIONAL ADVISORY COMMITTEE
FOR AERONAUTICS

WASHINGTON
September 30, 1948

NACA RM No. L8G20

NATIONAL ADVISORY COMMITTEE FOR AERONAUTICS

RESEARCH MEMORANDUM

EFFECT OF HIGH-LIFT DEVICES ON THE LOW-SPEED STATIC LATERAL AND YAWING STABILITY CHARACTERISTICS OF AN UNTAPERED 45° SWEPTBACK WING

By Jacob H. Lichtenstein

SUMMARY

A wind-tunnel investigation was made in the Langley stability tunnel to determine the effects of lift flaps (nose and split trailing edge) on the static lateral stability derivatives and the yawing derivatives of an untapered 45° sweptback wing at low speeds.

The results of the tests indicated that, in general, the addition of inboard trailing-edge split flaps tended to displace the curves for both the rolling moment due to yaw and the rolling moment due to yawing velocity negatively, whereas addition of 0.9-span outboard split flaps tended to displace the curves for both rolling moments positively. The addition of trailing-edge flaps tended, in general, to increase both the directional stability and the damping in yaw. Leading-edge flaps, however, generally caused the trends observed at low lift coefficients to extend to higher lift coefficients for the static lateral and yawing stability derivatives. The effect of flaps on either the lateral force due to yaw or the lateral force due to yawing velocity appeared to be unimportant. Because of the similar effect of the flaps on the derivatives due to yaw and yawing velocity, the effect of the flaps on the derivatives in yawing velocity appears to be indicated by the manner in which the flaps affect the derivatives in yaw.

INTRODUCTION

Estimation of the dynamic flight characteristics of airplanes requires a knowledge of the component forces and moments resulting from the orientation of the airplane with respect to the air stream and from the rate of angular motion of the airplane about each of its three axes. The forces and moments resulting from the orientation of the airplane usually are expressed as the static stability derivatives, which are readily determined in conventional wind-tunnel tests. The forces and moments related to the angular motions (rotary derivatives) have generally been estimated from theory because of the lack of a convenient experimental technique.

The recent application of the rolling-flow and curved-flow principle of the Langley stability tunnel has made equally possible the determination of both rotary and static stability derivatives, and this principle is now being utilized in a comprehensive program of research to determine the effects of various geometric variables on both rotary and static stability characteristics.

The results of an investigation of the static and yawing stability characteristics of a number of untapered swept wings, without high-lift devices, have been presented in reference 1. An investigation of the influence of fuselage and tail surfaces is reported in reference 2. The present investigation is concerned with the determination of the influence of various high-lift devices on the low-speed static lateral and yawing stability characteristics of one of the sweptback wings considered in reference 1. Inasmuch as the clean wing was compared to theory in reference 1, and no adequate theory for predicting the effect of flaps or sweptback wings is available, no comparisons between experiment and theory are made in this paper.

SYMBOLS

The results of the tests are presented as standard NACA coefficients of forces and moments, which are referred to the stability axes for which the origin is assumed at the projection on the plane of symmetry of the quarter-chord point of the mean aerodynamic chord of the wing of the model tested. The stability axes system is shown in figure 1 with positive forces and moments indicated. The coefficients and symbols used herein are defined as follows:

C_L	lift coefficient (L/qS)
C_X	longitudinal-force coefficient (X/qS)
C_Y	lateral-force coefficient (Y/qS)
C_l	rolling-moment coefficient (L'/qSb)
C_n	yawing-moment coefficient (N/qSb)
L	lift, pounds
X	longitudinal force, pounds
Y	lateral force, pounds
L'	rolling moment about X-axis, foot-pounds
N	yawing moment about Z-axis, foot-pounds

q dynamic pressure $\left(\frac{1}{2}\rho V^2\right)$

ρ mass density of air, slugs per cubic foot

V free-stream velocity, feet per second

S wing area, square feet

b wing span, feet

c chord of wing, measured parallel to plane of symmetry, feet

$\bar{c}$ mean aerodynamic chord, feet $\left(\frac{2}{S}\int_0^{b/2} c^2\,dy\right)$

x distance of quarter-chord point of any chordwise section from leading edge of root section measured parallel to plane of symmetry

$\bar{x}$ distance from leading edge of root chord to quarter chord of mean aerodynamic chord $\left(\frac{2}{S}\int_0^{b/2} cx\,dy\right)$

A aspect ratio (b^2/S)

Λ angle of sweep, positive for sweepback, degrees

ψ angle of yaw, degrees $(-\beta)$

β angle of sideslip, degrees

α angle of attack, measured in plane of symmetry, degrees

r yawing angular velocity, radians per second

$\frac{rb}{2V}$ yawing-velocity parameter

$$C_{Y_\psi} = \frac{\partial C_Y}{\partial \psi}$$

$$C_{n_\psi} = \frac{\partial C_n}{\partial \psi}$$

$$C_{l_\psi} = \frac{\partial C_l}{\partial \psi}$$

$$C_{L_\alpha} = \frac{\partial C_L}{\partial \alpha}$$

$$C_{Y_r} = \frac{\partial C_Y}{\partial \frac{rb}{2V}}$$

$$C_{n_r} = \frac{\partial C_n}{\partial \frac{rb}{2V}}$$

$$C_{l_r} = \frac{\partial C_l}{\partial \frac{rb}{2V}}$$

APPARATUS AND TESTS

The tests described herein were conducted in the 6- by 6-foot curved-flow test section of the Langley stability tunnel, in which curved flight may be simulated approximately by directing the air in a curved path about a fixed model. The methods and conditions of testing used to obtain the present data are described in reference 2.

The model used for these tests was an untapered wing with 45° sweepback and an aspect ratio of 2.61. The airfoil section was an NACA 0012 in a plane normal to the leading edge. The nose-flap chord was 10 percent of the wing chord and was fixed with the leading edge down 50°. The split trailing-edge flap was 20 percent of the wing chord and was deflected to an angle of 60°. The leading-edge flaps extended over the entire span, whereas the trailing-edge flaps extended over the outboard 90 percent of the semispan for one case and from 10 percent to 50 percent of the semispan for the other case. The 10 percent cutout at the center section in both cases was necessary to allow for the strain-gage mounting mechanism. (See figs. 2 and 3.) A photograph of the model in the tunnel is presented as figure 3.

The various test configurations are as follows:

Wing alone
Wing with nose flaps
Wing with 0.4-span split flaps
Wing with 0.9-span split flaps
Wing with nose and 0.9 span split flaps

The model was rigidly mounted on a single support strut at the quarter-chord point of the mean aerodynamic chord. The forces and moments were measured by strain gages. The moment strain-gage beams were mounted at the top of the strut, whereas the force units were placed along the strut below the moment gages. In order to mount the wing in this setup, a cutout was necessary so that the wing would fit around the moment beams. Clearance between the beams and the wing had to be maintained, and the resulting gap allowed some leakage to occur for which no correction was made.

Six-component measurements were made in straight flow through an angle-of-attack range which included from zero lift to beyond maximum lift at yaw angles of 0° and $\pm 5^\circ$. The pitching-moment data, however, were not considered reliable and consequently were not presented. The measurements of C_Y, C_n, and C_l in curved-flow tests were made only at $\psi = 0^\circ$. The tests were made with flow curvature which corresponds to values of $rb/2V$ of 0, 0.032, 0.067, and 0.088 for this model. All tests were made at a dynamic pressure of 25 pounds per square foot, which corresponds to a Mach number of 0.13 and a Reynolds number of 1.1×10^6 based upon the mean aerodynamic chord.

Results of check tests made on the clean wing were sufficiently close to those presented in reference 1 so that the data in reference 1 for the clean wing were used and were extended to lower lift coefficients by the addition of data from the present tests.

CORRECTIONS

Approximate corrections, based upon unswept-wing theory, for the effects of jet boundaries have been applied to the angle of attack, the longitudinal-force coefficient, and the rolling-moment coefficient. The lateral-force and yawing-moment coefficients have been corrected for the buoyancy effect of the static-pressure gradient associated with curved flow. (See reference 2.)

The values of C_{l_r} have been corrected for the tare associated with the induced load resulting from the presence of the strut for the wing at zero angle of attack. The same correction was applied throughout the angle-of-attack range.

No other tare corrections have been applied to the data. Corrections for the effects of blocking, turbulence, or the effects of static-pressure gradient on the boundary-layer flow have not been applied to these results. It is believed that omission of these corrections did not appreciably affect the results.

RESULTS AND DISCUSSION

Straight Flow

The lift and longitudinal-force characteristics for the clean wing and for the wing with the various flap configurations are presented in figure 4. The increase in maximum lift due to flaps are of the approximate order of magnitude expected on the basis of previous tests of similar configurations.

The change in the lift-curve slope for the nose-flap configurations which occurs at about zero angle of attack (fig. 4) is due to the spoiler effect of the nose flap on the air flow over the lower surface at low positive and negative angles of attack which is explained fully in reference 3.

The lateral static stability parameters $\left(C_{l_\psi}, C_{n_\psi}, \text{and } C_{Y_\psi}\right)$, which were determined during the course of the tests, were plotted against C_L, and these curves are presented in figures 5, 6, and 7. The addition of the nose flaps tended, in general, to delay until higher lift coefficients were attained the point at which the slope of the C_{l_ψ} curve appreciably decreased (fig. 5). The trailing-edge split flaps tended mainly to displace the C_{l_ψ} curve. The addition of the 0.9-span split flaps, which probably moved the lateral centers of pressure outboard, caused a positive displacement of the C_{l_ψ} curve. The 0.4-span split flaps, which probably moved the lateral centers of pressures inboard, caused a relatively small negative displacement of the C_{l_ψ} curve.

The values of C_{n_ψ} (fig. 6) for the flapped configurations generally were more negative than the values for the clean wing, and therefore greater directional stability for the flap configurations was indicated. It is interesting to note that for the flapped configurations, the model was directionally stable up to maximum lift. This increased stability can be attributed to the fact that the drag coefficient is larger for the flapped configurations than for the clean wing. When a sweptback wing is yawed with respect to the relative wind, the leading panel (left panel for positive yaw), which is at a smaller effective sweepback, has a greater velocity component normal to the leading edge than the trailing

panel and, consequently, a larger drag component. This drag differential between the two wing panels gives rise to a stabilizing yawing moment, and inasmuch as it is caused by a difference in velocity, it can be seen that this drag difference will be larger for larger drag coefficients.

Yawing Characteristics

The yawing velocity derivatives C_{Y_r}, C_{n_r}, and C_{l_r} were determined in the manner described in reference 2, which consisted of plotting C_Y, C_n, and C_l against $rb/2V$ for each angle of attack. The slope of a straight line faired through these points gives C_{l_r}, C_{n_r}, or C_{Y_r}.

The data for C_{l_r} plotted against C_L are presented in figure 8. The results for the clean wing are discussed in reference 1; however, it may be mentioned here that the break in the curve at C_L of about 0.5 is probably due to the early tip-stall characteristic of sweptback wings. In view of the fact that the forces at the tip, because of the longer arm, exert considerably more influence on the moment derivatives than forces near the center, it is easily understood why the tip stall should result in such a change in C_{l_r}. The fact that C_{l_r} breaks in a negative direction at lift coefficients above 0.5 indicates that the wing tip that is farther from the center of stream curvature begins to stall sooner than the wing tip that is nearer to the center of stream curvature. This probably is a result of the curved-flow field in which the wing is operating. For the present investigation, the model was mounted with the aerodynamic center on a radial line from the center of curvature; therefore, at this radial line all the streamlines are directed parallel to the X-axis when the model is at zero yaw. For points forward of the aerodynamic center the streamlines approach at effective negative yaw; whereas rearward of the aerodynamic center the streamlines approach at effective positive yaw. Inasmuch as the tips are rearward of the aerodynamic center, it could be said that the wing is effectively at positive yaw. Positive yaw tends to reduce the effective sweepback of the left wing panel and to increase it on the right panel. Because increased sweepback tends to delay the stall and since the left panel, which is farther from the center of rotation, stalls first, the rolling-moment curves therefore must break in a negative direction. The wing plus semispan trailing-edge-flap curve does not exhibit this decrease until the stall is more closely approached, and the curve in general is displaced negatively from the wing-alone results. The delay of the break in the curve is probably due to the fact that the semispan flaps increase the loading over the center part of the wing much more than at the wing tips and, consequently, the wing tends to exhibit somewhat more uniform stalling characteristics. Because of the high center-section loading, in order to obtain zero total lift, the angle of attack must be decreased

until the negative lift obtained at the tips is equal to the positive lift at the center. This effect, in combination with the spanwise velocity gradient under yawing conditions, should cause a negative displacement of C_{l_r} with respect to the clean wing. For the wing with 0.9-span outboard split flap configuration this condition is reversed; in this case the tips tend to load up more than the center with the consequence that the value of C_{l_r} at zero lift is positive with respect to the clean wing. Addition of nose flaps to either the wing alone or the wing with 0.9-span split flaps had only slight effect in the lift-coefficient range between zero and about 0.7. At the high lift coefficients, although the nose flaps were unable to prevent the break in the C_{l_r} curve, they did prevent an appreciable decrease in C_{l_r} until maximum lift was almost attained.

The damping-in-yaw characteristics C_{n_r} for the test configurations are presented in figure 9. The results show that addition of either nose flap or semispan trailing-edge flaps to the clean wing did not affect C_{n_r} over the range for which they are comparable. Addition of 0.9-span trailing-edge flaps or both nose and 0.9-span trailing-edge flaps considerably increased the damping in yaw $-C_{n_r}$. At high lift coefficients, the damping for the latter configurations was almost as much as that for a conventional model with a vertical tail. Although C_{n_r} is mainly a function of drag, for trailing-edge flap configurations where the center of pressure is considerably rearward of normal, the side force also can influence C_{n_r}. This effect can be observed for both the wing with 0.9-span split flaps and the wing with nose and 0.9-span split-flap configurations by noting that where the C_{Y_r} curve (fig. 10) was somewhat positive with respect to the clean wing, the C_{n_r} curve for the flapped configurations was considerably more negative than the clean wing.

The magnitude and variation of C_{Y_r} with lift coefficient for the wing was so small that it is believed to be of slight significance (fig. 10) and the addition of flaps did not appreciably alter these characteristics.

An interesting general observation that can be made is the very similar manner in which the flaps affect the static lateral stability derivatives $\left(C_{l_\psi}, C_{n_\psi}, \text{ and } C_{Y_\psi}\right)$ and the corresponding yawing stability derivatives $\left(C_{l_r}, C_{n_r}, \text{ and } C_{Y_r}\right)$. This seems to indicate that the manner in which flaps are likely to affect the yawing stability derivatives of a wing configuration can be predicted by observing the effect the flaps have on the static stability derivatives of the wing.

CONCLUSIONS

Tests of a 45° sweptback untapered wing with lift flaps in straight and yawing flow indicate the following general conclusions:

1. At a given lift coefficient, the curves of rolling moment due to yaw and rolling moment due to yawing velocity were, in most instances, displaced negatively by the addition of inboard trailing-edge split flaps and displaced positively by the addition of 0.9 span outboard trailing-edge split flaps.

2. Trailing-edge split flaps were generally found to increase the directional stability and the damping in yaw.

3. Leading-edge flaps generally cause an extension to higher lift coefficients of the trends usually noted at low lift coefficients for the static lateral and yawing stability derivatives.

4. Because of the similar effect of the flaps on the derivatives due to yaw and yawing velocity, the effect of the flaps on the derivatives in yawing velocity appears to be indicated by the manner in which the flaps affect the derivatives in yaw.

5. The effects of flaps on either the lateral force due to yaw or the lateral force due to yawing velocity appear to be unimportant.

Langley Aeronautical Laboratory
National Advisory Committee for Aeronautics
Langley Field, Va.

REFERENCES

1. Goodman, Alex, and Brewer, Jack D.: Investigation at Low Speeds of the Effect of Aspect Ratio and Sweep on Static and Yawing Stability Derivatives of Untapered Wings. NACA TN No. 1669, 1948.

2. Bird, John D., Jaquet, Byron M., and Cowan, John W.: Effect of Fuselage and Tail Surfaces on Low-Speed Yawing Characteristics of a Swept-Wing Model as Determined in Curved-Flow Test Section of Langley Stability Tunnel. NACA RM No. L8G13, 1948.

3. Fullmer, Felicien F., Jr.: Two-Dimensional Wind-Tunnel Investigation of the NACA 64_1-012 Airfoil Equipped with Two Types of Leading-Edge Flap. NACA TN No. 1277, 1947

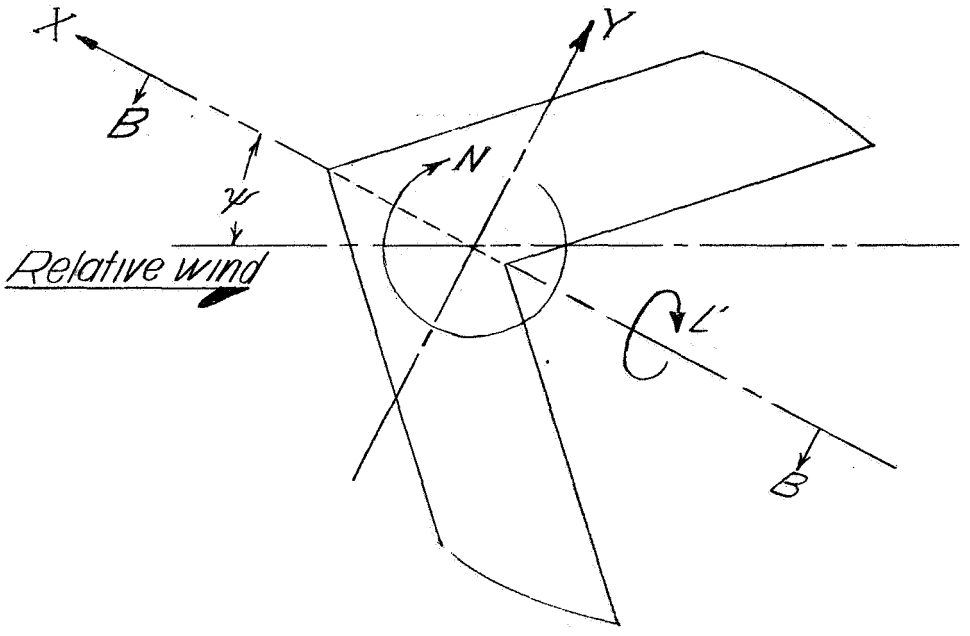

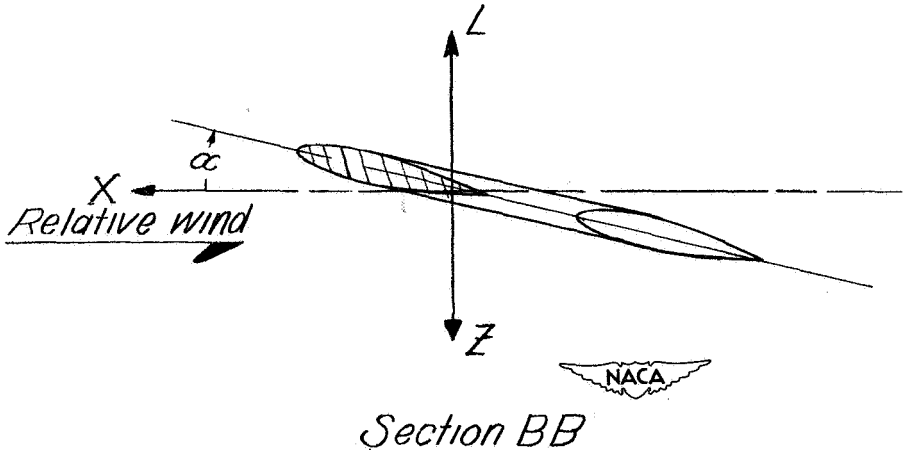

Section BB

Figure 1.- System of axes used. Positive values of forces, moments, and angles are indicated.

$A = 2.61 \quad S = 3.56\ ft^2 \quad b = 3.05\ ft \quad \bar{x} = 1.05\ ft$

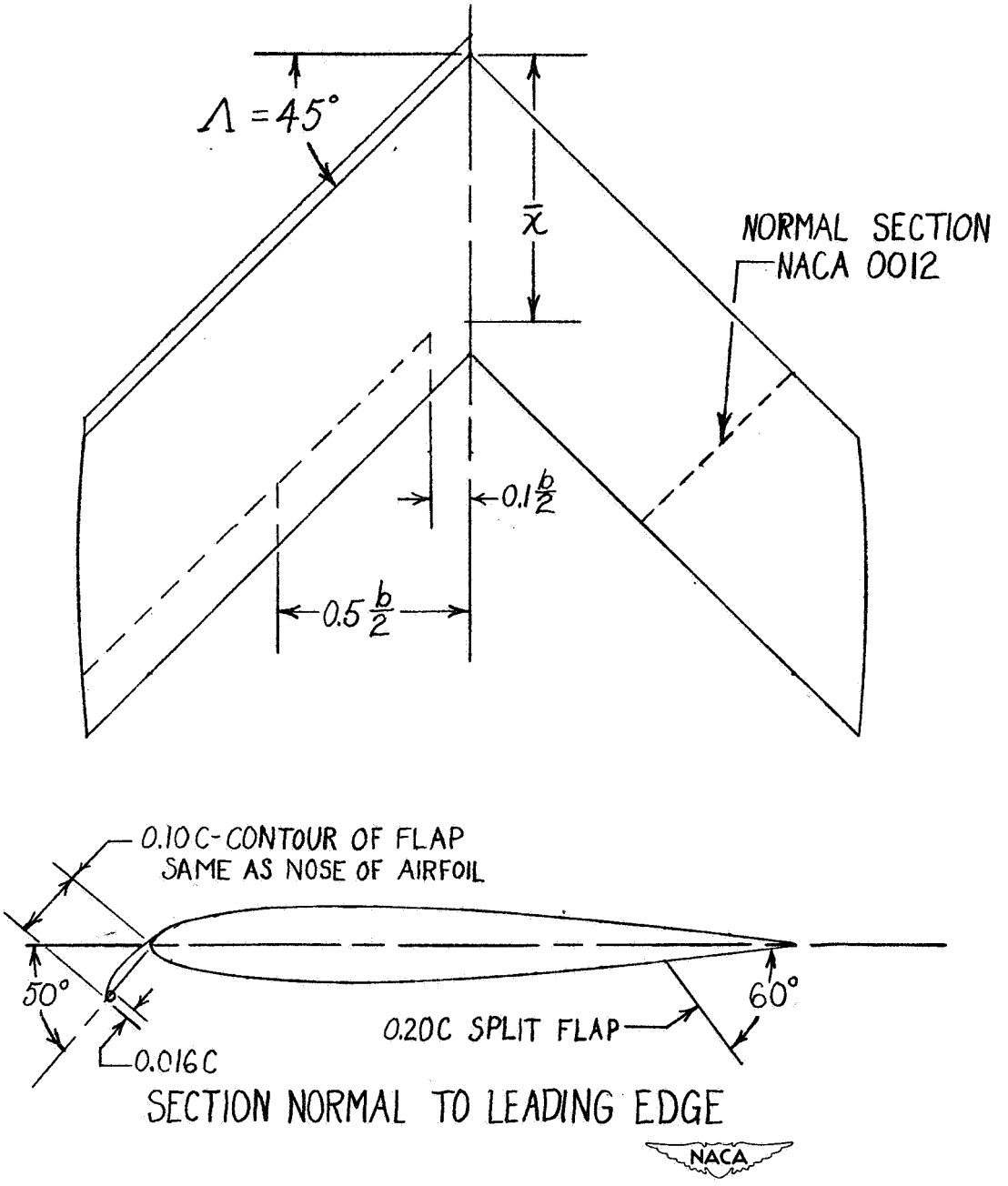

Figure 2.- Sketch showing model in the configurations tested.

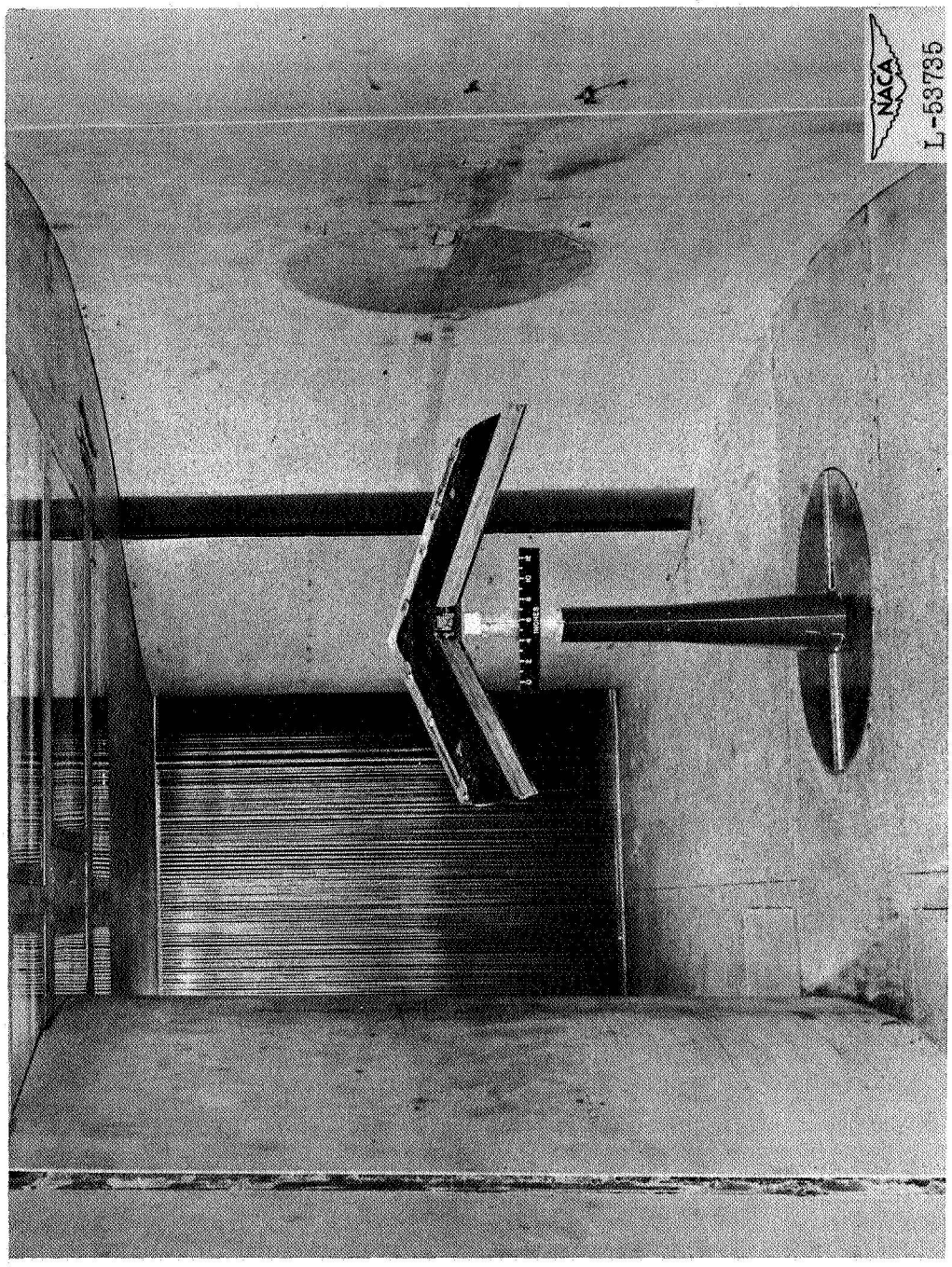

Figure 3.- Wing with nose and trailing-edge flaps mounted on the strain-gage strut in curved-flow test section of the Langley stability tunnel. Model mounted inverted; looking upstream.

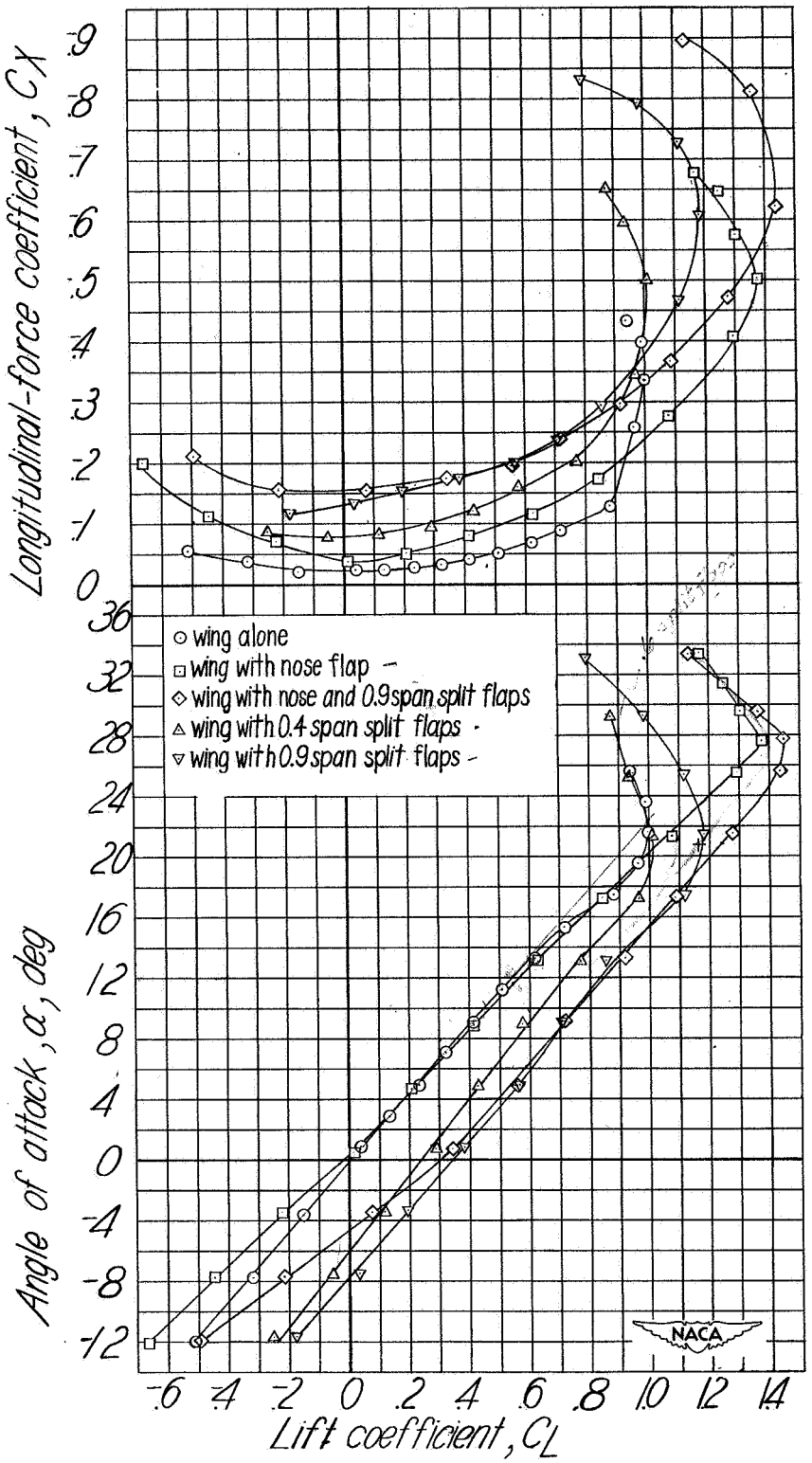

Figure 4.- Variation of angle of attack and longitudinal-force coefficient with lift coefficient for various test configurations.

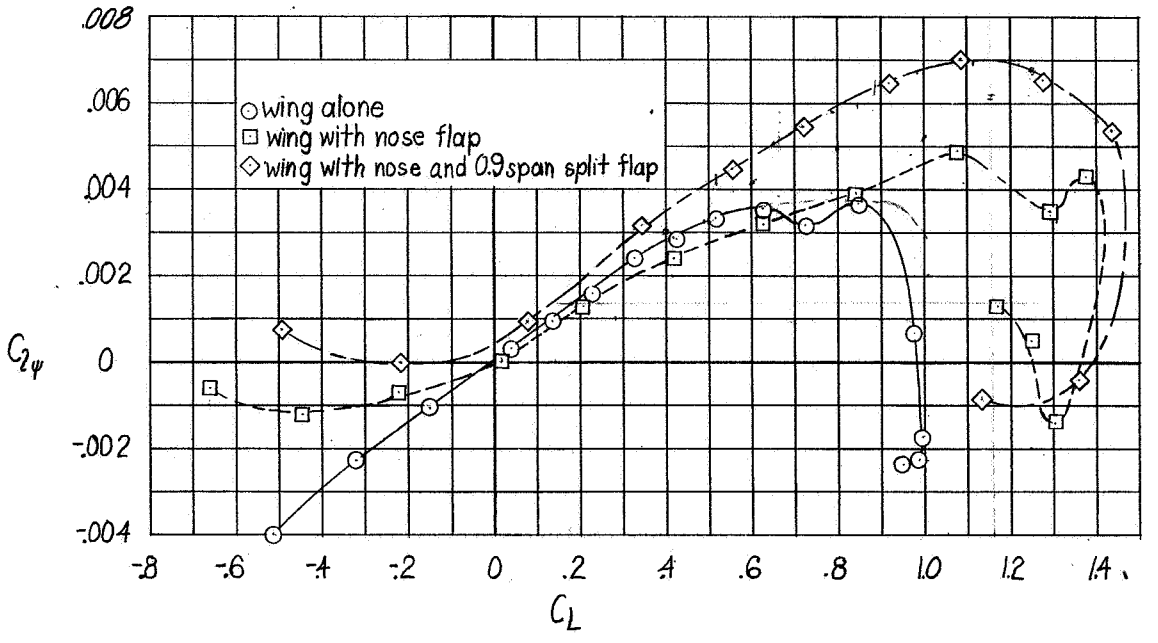

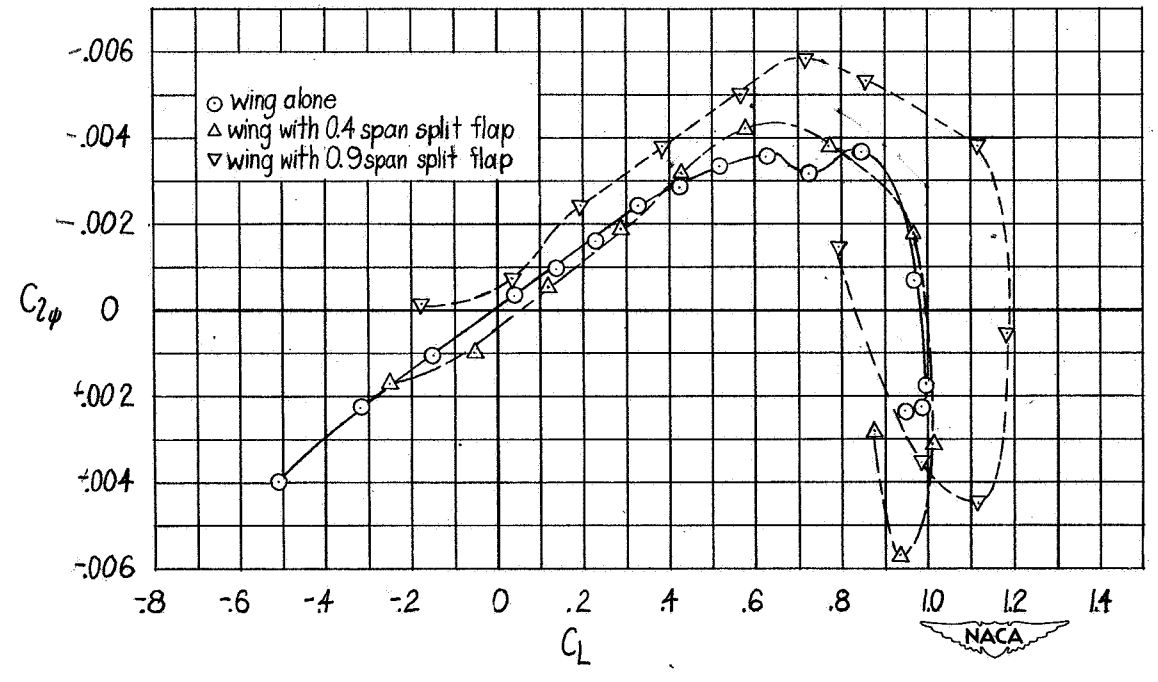

Figure 5.- Variation of C_{l_ψ} with lift coefficient for the various test configurations.

C_L 1.24
α = 13.2°

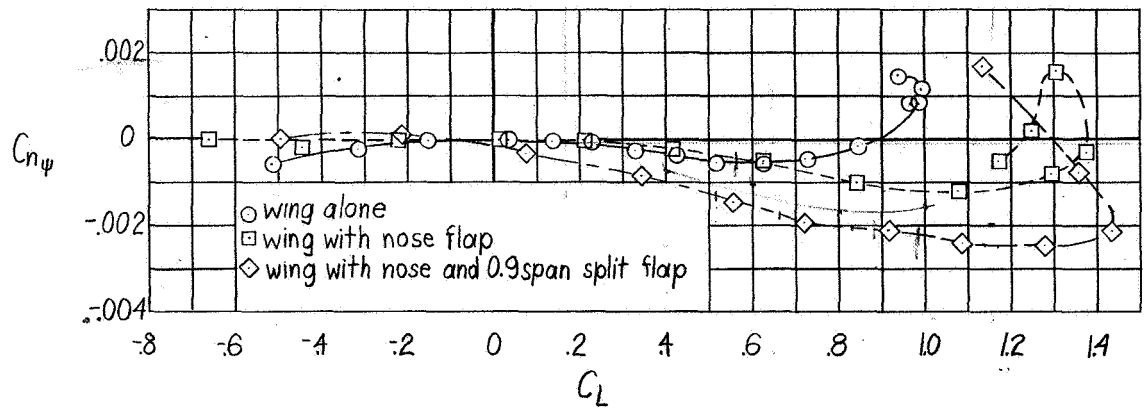

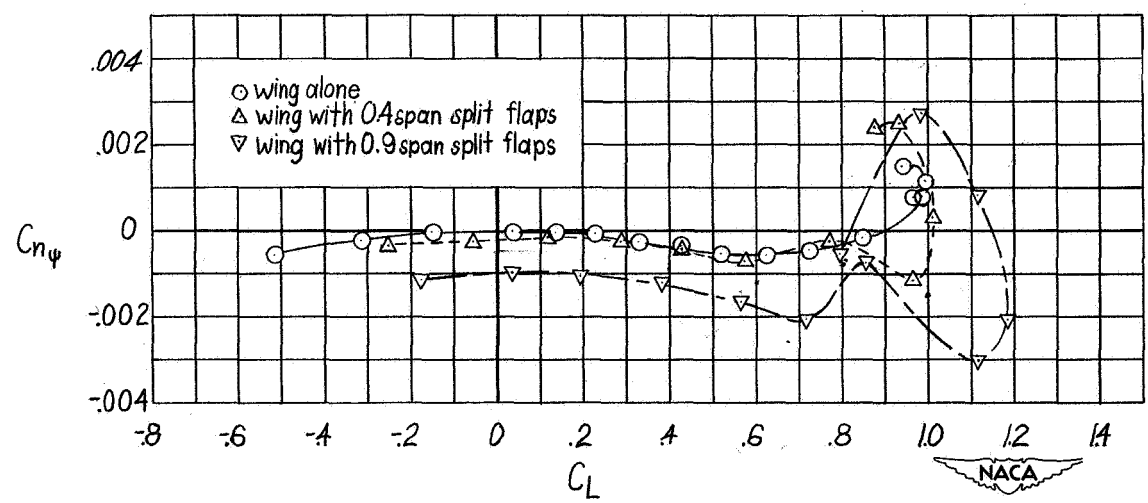

Figure 6 - Variation of C_{n_ψ} with lift coefficient for the various test configuration.

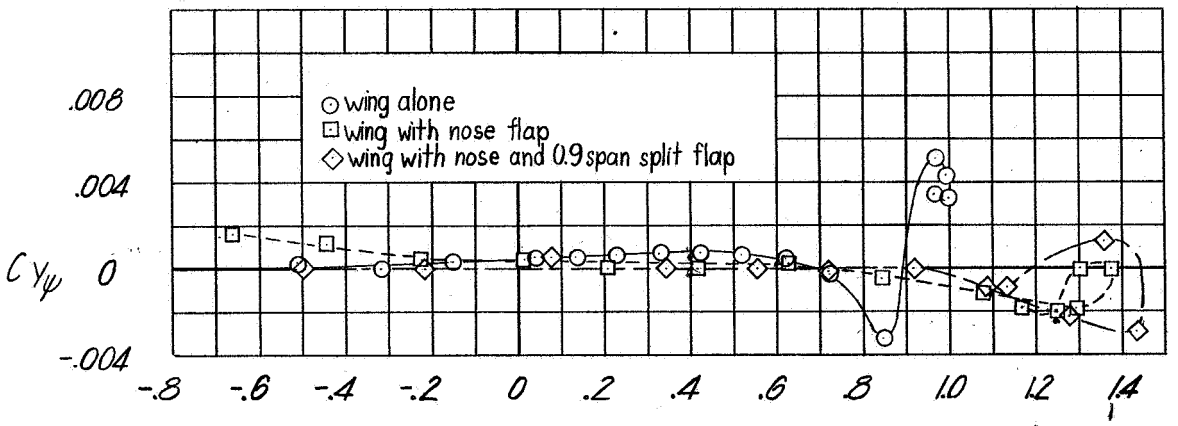

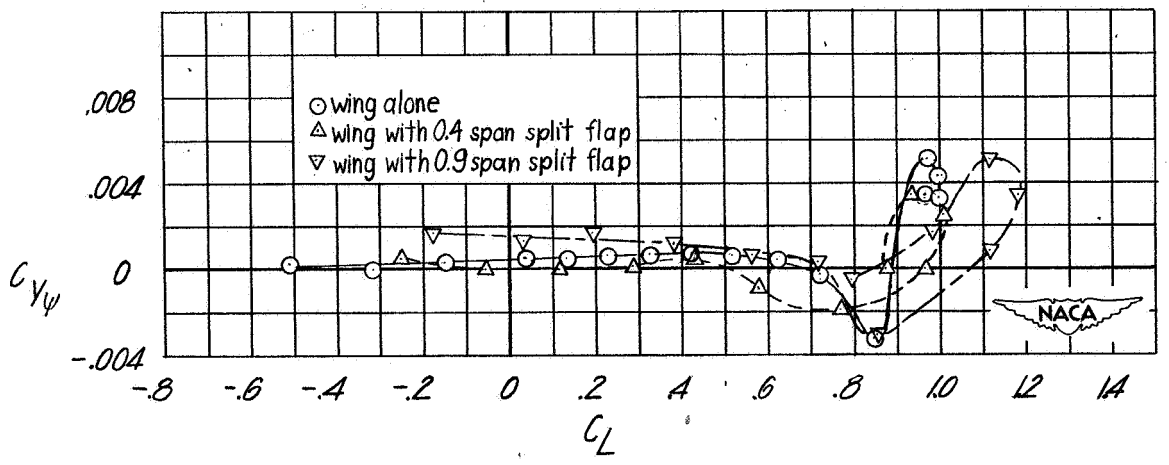

Figure 7.- Variation of C_{Y_ψ} with lift coefficient for the various test configurations.

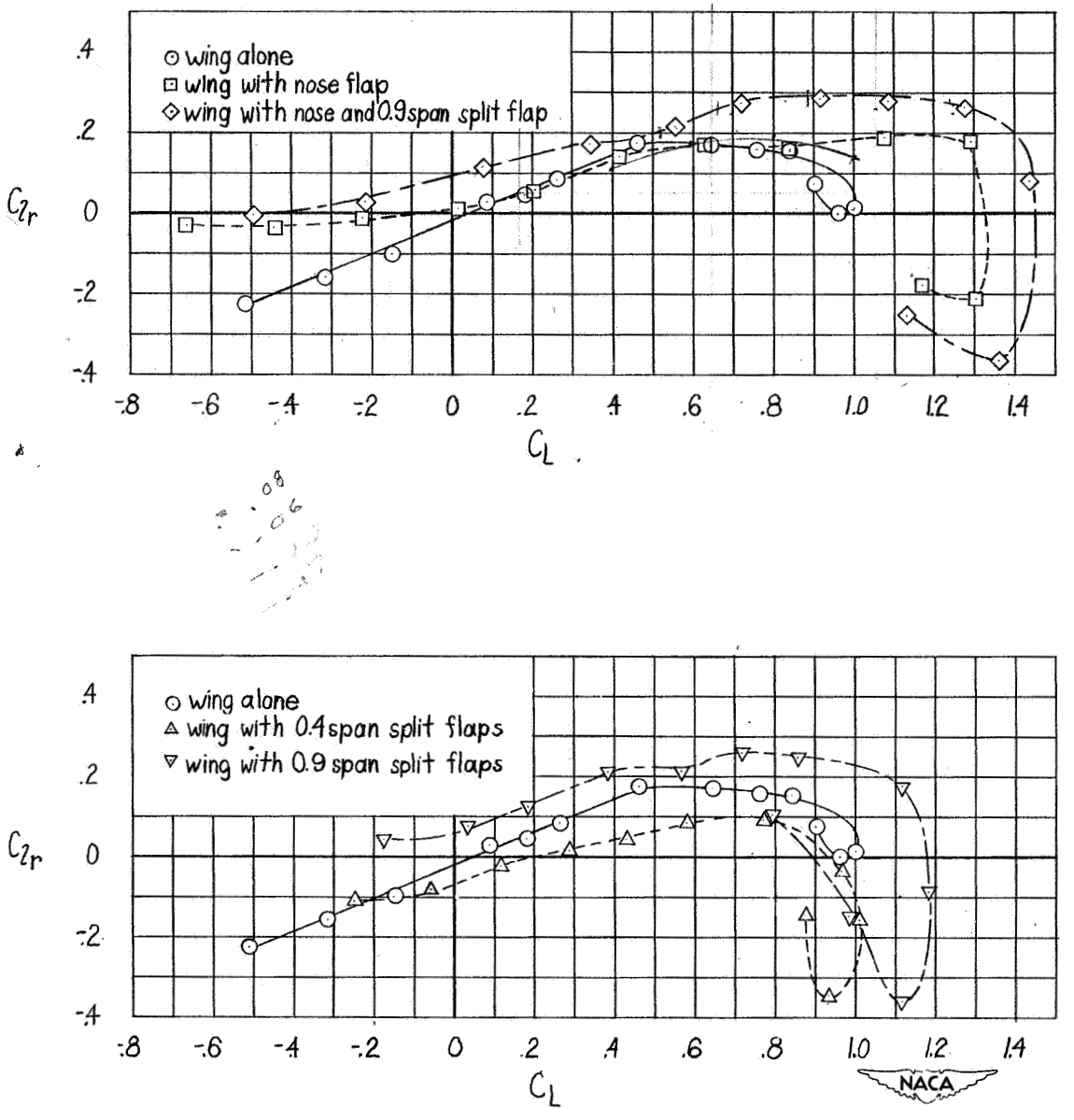

Figure 8.- Variation of C_{l_r} with lift coefficient for the various test configurations.

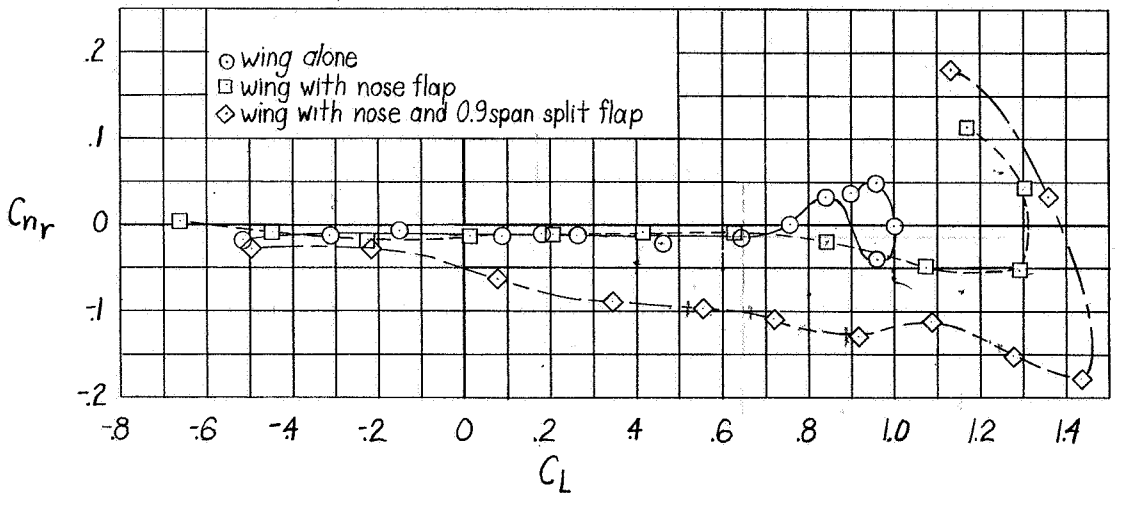

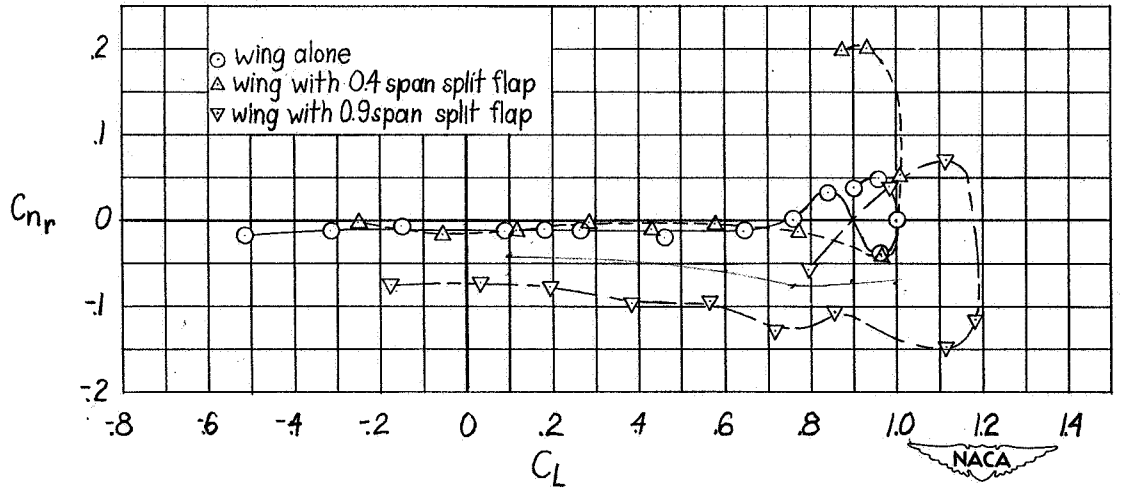

Figure 9.- Variation of C_{n_r} with lift coefficient for the various test configurations.

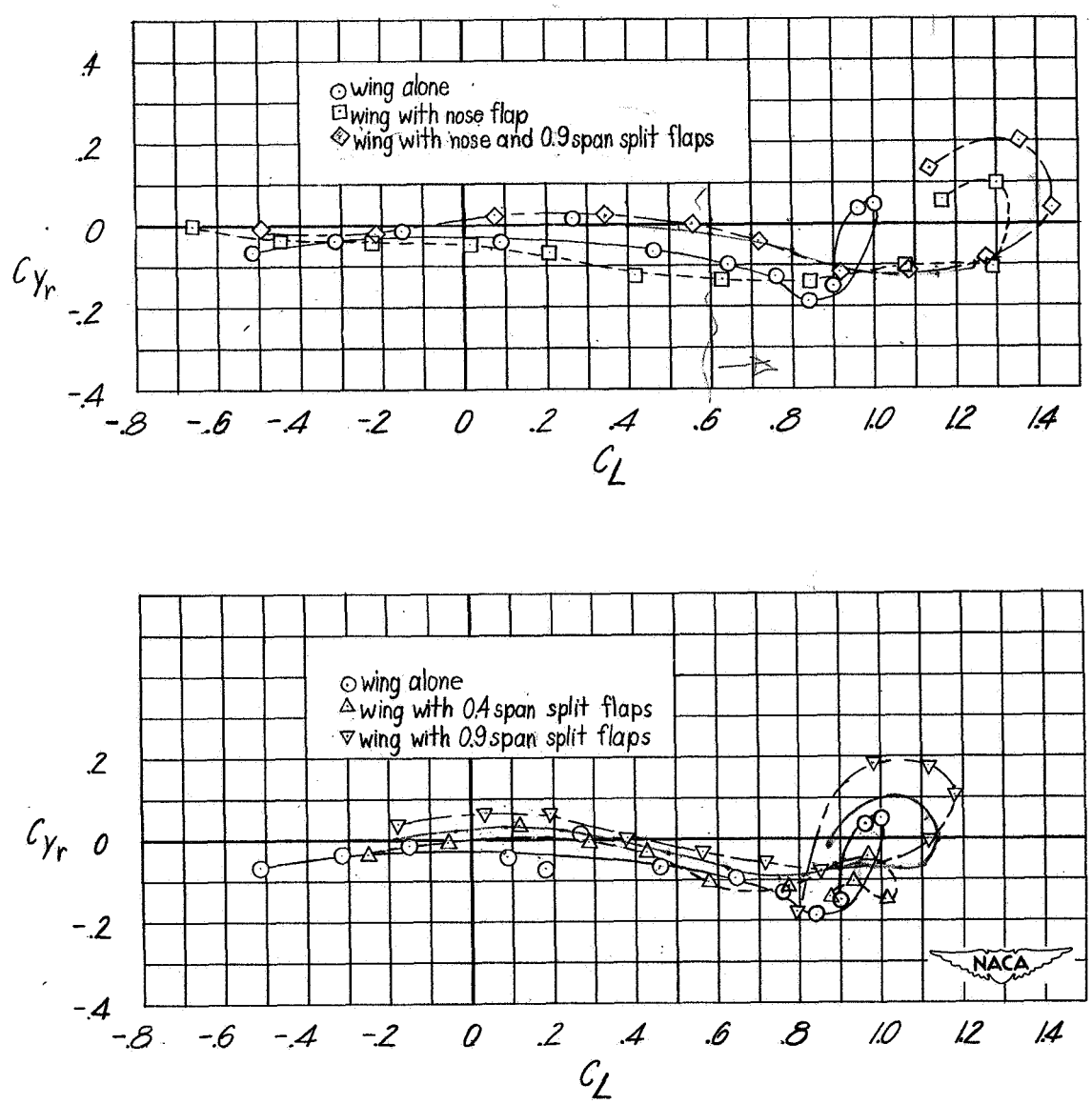

Figure 10.- Variation of C_{Y_r} with lift coefficient for the various test configurations.